8-2021

Acoustic Parameters as Discriminators of Wall Events in PICO Dark Matter Search Data

Lucia Volkova
Northeastern Illinois University, lvolkova@neiu.edu

Recommended Citation

Volkova, Lucia, "Acoustic Parameters as Discriminators of Wall Events in PICO Dark Matter Search Data" (2021). *University Honors Program Senior Projects*. 26.
https://neiudc.neiu.edu/uhp-projects/26

ACOUSTIC PARAMETERS AS DISCRIMINATORS OF WALL EVENTS IN PICO DARK MATTER
SEARCH DATA

A Thesis Presented to
the Faculty of the University Honors Program
Northeastern Illinois University

In Partial Fulfillment of the Requirements
of the NEIU Honors Program
for Graduation with Honors

LUCIA VOLKOVA

August, 2021

HONORS SENIOR PROJECT

ACCEPTANCE AND APPROVAL FORM

Lucia Volkova

Acoustic Parameters as Discriminators of Wall Events in PICO Dark Matter Search Data

This thesis has been reviewed by the faculty of the NEIU Honors Program and is found to be in good order in content, style, and mechanical accuracy. It is accepted in partial fulfillment of the requirements of the NEIU Honors Program and graduation with honors.

_____

Dr. Orin Harris, Department of Physics   Date
Faculty Advisor

_____

Prof. Paulo Acioli, Department of Physics   Date
Faculty Reader

_____

Prof. Denise Cloonan Cortez de Andersen, Department of World Languages and
Cultures   Date
Honors Curriculum & Standards Board

_____

Prof. Jon B. Hageman, Department of Anthropology   Date
Coordinator, University Honors Program

ABSTRACT

Bubble chambers are one of several detector types that particle physicists use to search for the as-yet-undetected dark matter. The PICO collaboration – formed from the merger of the similar PICASSO and COUPP experiments – runs such a bubble detector using superheated fluorocarbons (with and without iodine). Bubbles that form along chamber walls exhibit different behavior than those which nucleate in the bulk of the target liquid due to shape distortions from the wall boundary; in previous analyses when searching for dark matter, these wall events have been cut from the data to control for the differing behavior using information available from images or pressure rise data. Seventy-nine events of dark matter search data acquired by the PICO-60 bubble chamber in 2016 were visually categorized as wall or bulk events and analyzed acoustically. Wall events were found to significantly differ from bulk events using multiple acoustic parameters including overall loudness. Acoustic data was found to be a promising indicator of event type and yielded an efficient and reliable fiducial cut (100% specificity with up to 92% efficiency), likely allowing for a larger volume of target fluid to be considered in future analyses. Having multiple modes of observation is also critical in validating existing methods of fiducialization. The preliminary results indicate that future analyses would likely showcase several percent more efficient fiducialization by leveraging acoustic handles similar to those investigated here.

ACKNOWLEDGEMENTS

TABLE OF CONTENTS

LIST OF FIGURES

INTRODUCTION

Dark matter is one of the most mysterious concepts in physics today; it is a substance which we believe to account for ~85% [1] of all the mass in the universe, yet we have not observed it directly on small scales, nor do we know what dark matter is. What we do know is that while dark matter does not interact with electromagnetic radiation (e.g., visible light and is therefore 'dark' – though more accurately described as invisible), it does interact with the gravitational field. This is how we came to know of its existence; large-scale structures in the universe such as spiral galaxies do not have enough ordinary, observable mass to account for their speed of rotation – under our currently understood gravitational theory, they should be flying apart. Similarly, the velocity dispersion, which measures the spread in velocities of constituent objects (stars or galaxies) relative to the average velocity of the group (elliptical galaxy or galaxy cluster, respectively), is also correlated with the distribution of a dark matter halo around these structures; more dark matter means more gravity to keep constituent objects tightly bound. Einstein's general relativity, which posits that gravitational fields of massive objects will deflect light, can be used to measure the mass of obscuring objects based on how much they bend the light coming from other, more distant objects behind them. This phenomenon is known as gravitational lensing (see Figure 1), and it has been used to deduce that the masses of many of these

Figure 1. Gravitational lensing (circular arc) of background galaxy by central elliptical galaxy

gravitational lenses (galaxies, globular clusters, etc.) are too great to be accounted for by visible, baryonic matter alone. Baryonic matter is the material with which we are familiar: protons, neutrons, electrons.

Today, the most precise evidence for the existence of dark matter is provided by the cosmic microwave background (CMB – see Figure 2) [1]. This radiation is a remnant of the Big Bang, in which the universe was initially extremely hot and dense and full of baryonic matter coupled with photons undergoing density oscillations. About 380,000 years later, the universe expanded and cooled enough for decoupling to occur; stable atoms could form and photons – providing a view of the early universe and encoding density information – could travel freely through the universe to reach our observatories today, revealing profound cosmological details such as the geometry and composition of the universe [2]. Cosmic microwave background measurements strongly suggest the presence of a substantial amount of some non-baryonic matter in the early

universe. This matter affected the density oscillations by exerting an inward gravitational pull but without the usual resulting pressure increase and balancing outward force that would be present with ordinary matter. Between the CMB measurements and our observations of velocity and mass distributions, we have enough evidence to
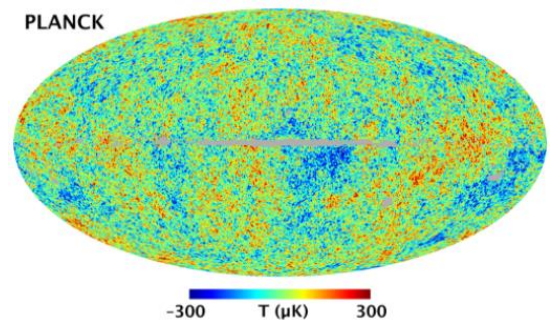

Figure 2. Sky map from Planck satellite showing anisotropies (temperature variations) of cosmic microwave background (CMB) [3]

conclude with confidence that most of the "stuff" in the universe has yet to even be identified.

BUBBLE CHAMBERS & PICO COLLABORATION

The leading candidate to explain dark matter is an as-yet-undiscovered elementary particle called a WIMP (weakly interacting massive particle) [4]. Other theorized candidates include certain types of neutrinos, axions (similar to photons but with a miniscule mass), MACHOs (massive astrophysical compact halo objects, such as neutron stars and brown dwarfs), and MOND (modified Newtonian dynamics) theories which seek to revise our understanding of gravity to fit observations. Of these, WIMPs are the leading candidates due to the number of observations their existence could explain [5]. In an attempt to search for these possible dark matter candidates, physicists around the globe have been building ever larger and more sensitive detectors. One detector type is called a bubble chamber – invented in the 1950s by Donald Glaser, which awarded him the Nobel Prize in Physics in 1960. A bubble chamber is a sealed vessel filled with some superheated (and transparent, for photographical purposes) liquid. This superheated liquid is unstable and just above its boiling point. Any energy deposition into a small enough area in the chamber, such as from that of background radiation, neutrinos, or – theoretically – dark matter particles colliding with the molecules of the liquid, can nucleate a bubble which will rapidly expand, causing the liquid in the chamber to boil. Trails of multiple bubbles are also possible. The chamber is outfitted with measuring devices to capture visual, acoustic, temperature, and pressure data associated with each event. Repeated enough times, with enough data, we can

begin to analyze and comment on the likely sources of the bubbles that are observed, and the probabilities that the events we are seeing are caused by this elusive dark matter. This research will focus on acoustic data, which can reveal information about the particle collision that produced it and perhaps the location of the event, including the proximity of the event to the chamber wall, allowing for more precise future analyses. These analyses currently rely on visual fiducialization (the identification of the inner, uncontaminated volume of the detector).

Various other detector types are in use today as well [6]. Some use scintillating crystals such as sodium iodide or liquid noble gas such as xenon as the target material. Others use cryogenic bolometers which can measure the power of incident particles due to the temperature increase they produce, as the bolometer includes a material with temperature-dependent electrical resistance. Each detector has pros and cons; the primary advantage of bubble chambers as dark matter detectors is that we are able to fine-tune the

Figure 3. Schematic of PICO-2L bubble chamber [4]

pressure and temperature within the target fluid to specify the types of particle interactions to which the detector is sensitive. This allows bubble chambers to not be sensitive to electron recoils, which is the primary type of background event seen in
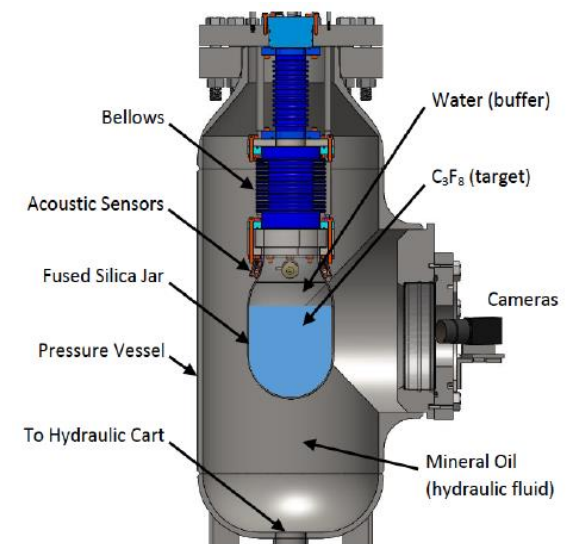
many other experiments. More on background radiation and how it is accounted for is discussed in later paragraphs.
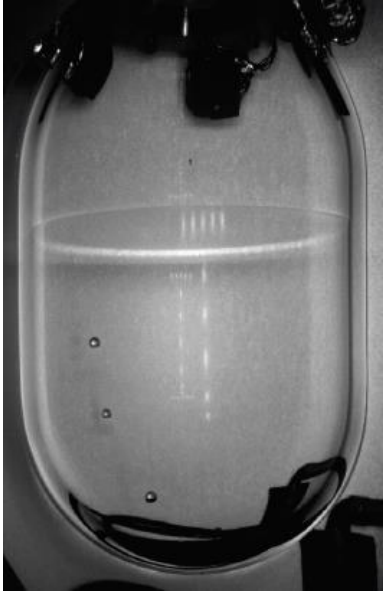

Figure 4. Nucleated bubbles in 4kg PICO chamber

The PICO bubble chambers (named after the merger of PICASSO and COUPP collaborations) in Canada's SNOLAB – located in Sudbury, Ontario – are at a depth of around 6,000 meters water equivalent (MWE) underground (2km) [7, 8, 9]. While the experiments began with a 2-liter-target chamber [10, 4], they have expanded over the years. In 2015, PICO-60 was the largest operational dark matter bubble chamber on Earth. Design of a 500-liter chamber to be located at SNOLAB is currently underway. The main components of the PICO-60 chamber include a 1-meter by 0.3-meter fused silica jar which is sealed to a stainless-steel bellows that transmits pressure from the surrounding vessel into the active volume. The jar is where the superheated target fluid (C_3F_8 or CF_3I) and pure water buffer are held, and the jar-bellows construction is inside of a 1.67 m by 0.6 m stainless-steel pressure vessel filled with hydraulic fluid (propylene glycol or mineral oil). The water buffer is added to prevent the superheated fluid from coming into contact with and possibly becoming contaminated by the steel bellows; however, newer prototypes of PICO chambers are coming online that do not use buffer fluids [11]. The entire pressure vessel setup is submerged in a 3.7 m by 2.9 m water tank to shield the target fluid from neutron radiation, and all of these components are in thermal contact, ensuring the detector is

in equilibrium at a set temperature (see Figure 3 for a diagram). Thirteen piezoelectric acoustic transducers are epoxied to the bell jar exterior to measure acoustic signals from bubble nucleation events within the chamber and two to four CMOS cameras (those with Complementary Metal-Oxide Semiconductor sensors) are used to photograph the inside of the chamber in stereo, allowing for triangulation of a bubble's position within the chamber to within ~1 cm accuracy.

A run cycle begins when the pressure in the external hydraulic cart is lowered to somewhere between 20 and 55 psia in approximately 5 seconds. This is referred to as the "expanded" state where the target fluid is superheated, and the chamber is kept in this state for at least 25 seconds before data collection begins – ensuring any bubble nucleation events are not a result of the chamber expansion. Image data from the cameras is the primary trigger for an event; differences between consecutive frames indicating the presence of a growing bubble initiate a piston compression to stop the liquid from boiling. Along with the images, acoustic data, pressures, and temperatures are logged during the entire event. Once an event is triggered, the pressure is increased to take the fluid out of a superheated state and recondense any vapor. The hydraulic cart is capable of raising the pressure to approximately 200 psia within 250 ms. This hydraulic system is quite loud, so acoustic data from the piezos can reasonably be cut out once the voltage passes a certain threshold and it is assumed the sound is coming from chamber operation rather than bubble nucleation. The acoustic data is primarily used to reject bubbles produced by radioactive alpha-decay, and will later be described in more detail.

Analysis of results and sensitivity of the bubble chamber to dark matter depends on the theoretical model used to explain bubble nucleation and the calibration data used to verify the model. The pressure and temperature of the target fluid will
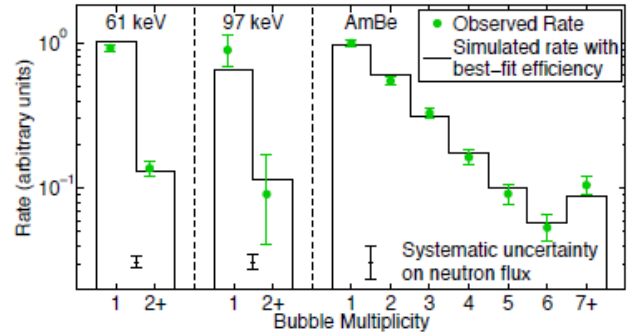

Figure 5. Green points show observed rates while black histograms show simulated rates predicted for neutron bubble nucleation. Data from 61 keV, 97 keV, and AmBe source. [4]

determine the conditions for radiation-induced nucleation. The Seitz "hot spike" model is used to approximate the minimum energy deposition needed within a given critical radius for bubble nucleation to occur. In this model, a particle that deposits an amount of energy greater than this Seitz threshold into the critical radius will nucleate a bubble with 100% efficiency. Neutron calibration data have shown that this model is inaccurate, as we do not observe perfectly efficient nucleation above this threshold in CF_3I. The reason for this has been found to be that carbon and fluorine atoms in this target fluid produce recoil tracks which are often larger than the critical bubble diameter [7]. Iodine recoils, having much shorter tracks, nucleate bubbles far more consistently compared to fluorine. In C_3F_8, however, fluorine *does* nucleate efficiently – its tracks are shorter in that fluid. Such results typically refer to events occurring in the bulk of the fluid, but events occurring along the chamber walls can also differ from non-wall events in that

bubbles are obstructed and cannot become completely spherical; here the Seitz energy threshold is also not expected to model bubble nucleation well.

Unable to rely on the Seitz model alone to determine nucleation efficiency, neutron calibration runs were carried out in the PICO chamber using *AmBe* and *YBe* neutron sources. Neutrons from these radioactive materials interact with the nuclei of atoms in the target fluid, nucleating bubbles. A single neutron can result in more than one interaction, yielding a chain of bubble events; the more bubbles per event, the higher the nucleation efficiency. The rate of bubbles (and bubble groups) observed are compared to a simulated rate using the Stopping Range of Ions in Matter (SRIM)
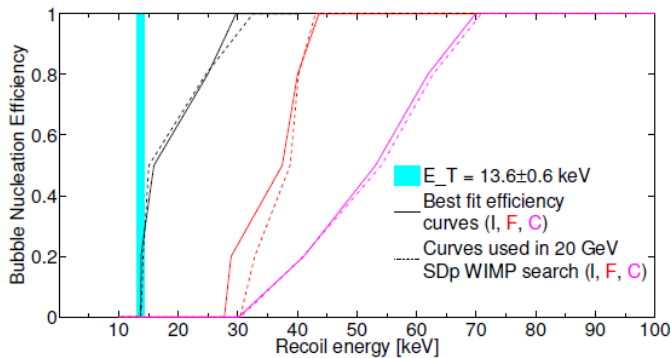

Figure 6. Best fit efficiency curves (solid) for iodine, fluorine, and carbon at 13.6 keV Seitz threshold along with curves chosen (dashed) to search for 20 GeV spin-dependent WIMP. [7]

software package. A comparison of observed versus simulated rates for data from two energies and the *AmBe* source is shown in Figure 5. This neutron calibration is then used to constrain sensitivity to fluorine and carbon (and iodine, in the case of CF_3I)

recoils. Using the efficiency curves such as in Figure 6, sensitivity to a particular dark matter particle is calculated (WIMP of a given mass and coupling). For the sake of being conservative, a combination of efficiency curves is chosen such that the *least* sensitivity is provided.

Several catalysts for bubble nucleation are known which are more probable than dark matter interactions, and much effort goes into minimizing these sources and measuring/discriminating against that which remains. Microscopic imperfections in the silica jar, material radioactivity, as well as transient thermodynamic effects during expansion and compression of the chamber can nucleate bubbles. These effects are minimized by using high-quality materials and allowing the chamber to settle and remain stable for ~25 seconds prior to data collection. Most of the remaining sources of potential bubble nucleation are external background radiation in the form of alpha, beta, gamma, or neutron particles.

Alpha particles are helium nuclei (two protons, two neutrons) and often have kinetic energies around 5 MeV. They can be produced spontaneously via alpha decay such as that of radon in the air or be the result of cosmic rays. Cosmic rays are mitigated by the thousands of cubic meters of rock surrounding the apparatus, while pressures and temperatures within the chamber are tuned such that decays with typical alpha particle energies are discriminated against acoustically. Alpha recoils are fairly easy to identify by the PICO detector, as they are several times louder than other backgrounds [4]. This is due to their much larger relative track length. Sound emission has been shown to peak when bubbles are roughly 20 µm in diameter. Alpha particles deposit their energy over a longer distance (~40 µm); however, the energy deposition is still larger than the Seitz threshold, meaning that multiple nucleation sites will result in an overall acoustic signal louder than that of events with only one nucleation site.

Beta radiation is composed of high-speed electrons or positrons emitted by atomic nuclei undergoing beta decay. Electron recoils are often on the order of around 1 keV, which the detector can also discriminate against. This is done by adjusting the pressure and temperature of the target fluid such that the longer tracks left by electrons do not deposit enough energy per unit length to nucleate bubbles; electron recoils are rendered invisible to the detector [12]. Gamma radiation results in electron recoils as well and is thus discriminated against. Neutron radiation often results in multiple recoil events, and therefore, multiple bubbles that can be visually identified. We expect bubbles from WIMP candidates to look – but not sound – like alpha decay bubbles or single neutron recoil event bubbles.
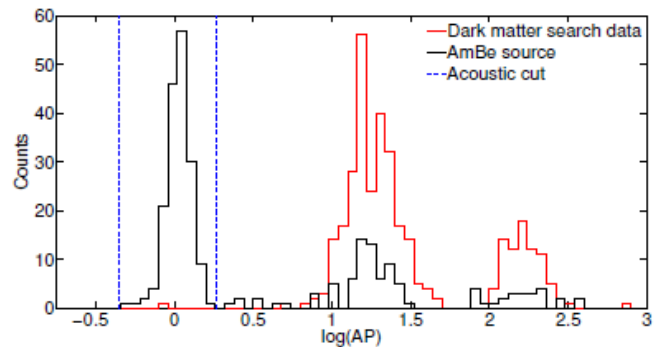
Figure 7. AP distributions for neutron calibration (black) and WIMP search data (red). Single nuclear recoils are between the dashed lines; the two peaks at higher AP, for both calibration and dark matter data, are from Radon alpha decay chains.

PREVIOUS PICO RESULTS

The data undergo a series of cuts prior to data analysis. This is done to ensure that the sample used for dark matter searches is controlling for as many other variables as possible. A fiducial volume cut is defined on neutron calibration data to eliminate wall events – which are far more numerous than bulk events, per Figure 9 – and this has

previously been done using optical and fast pressure rise data. The assumption is made that dark matter events will be randomly distributed throughout the target fluid volume, and statistical analysis of the spatial distribution of events can test for the radius (from jar center) at which the event distribution ceases to be uniform. However, there is an upper limit on the accuracy of optical data for this purpose, as spatial resolution can only be improved so much. Events typically within ~5 mm of the jar wall are removed from the analysis to ensure that any observed acoustical differences are not the result of bubbles forming along the wall; the acceptance of this fiducial cut was 0.90 ± 0.01 by volume for PICO-60 and 0.82 ± 0.01 for PICO-2L (increasing to 0.92 ± 0.02 for pressure rise data-based derivations). Improvement in the efficiency of this particular cut using independent acoustic data as well as reduction in the false positive rate of wall event identification are the main goals of this research. Additional cuts are applied to eliminate those events with excessive acoustic noise as well as events whose time of bubble formation is outside of the expected range. The acceptance of these cuts is dependent on pressure and varies from 0.89 to 0.94 ± 0.02, as the acoustic signal-to-noise ratio decreases with increasing pressure.

Acoustic parameters (AP) are used to characterize the power of a bubble nucleation event. The acoustic signal is divided into frequency bands which are then corrected for the pressure, temperature, and bubble position within the chamber; then the AP distributions are normalized. In PICO-60, two parameters are used in the analysis: the low acoustic parameter (AP_{low}) is the sum of normalized frequency bands between $7 - 63$ kHz, while the high acoustic parameter (AP_{high}) is the sum from

frequencies between 63 – 110 kHz. Plotting a histogram of event count versus the natural log of AP shows peaks on the higher side of the acoustic parameter scale (for both low and high AP) which correspond to alpha decay events. Using AP_{low}, a clear cut can be identified to discriminate alpha decays from nuclear recoils (see Figure 7). AP_{high} was used to investigate the properties of a group of "mystery" background events from the PICO-60 CF_3I search results.

The multiple alpha peaks and loudness of these events is supported by our understanding of the decay of Radon-222. When this atom undergoes decay, the result is an alpha particle (5.48 MeV) and daughter atom of Polonium-218. Soon after (having a half-life of ~3 mins), this isotope alpha-decays yet again (6.0 MeV) into an atom of Lead-214. Within an hour, the atom will most likely have undergone beta decay before becoming Polonium-214. This polonium isotope undergoes a third and final alpha decay (7.68 MeV) – the most energetic of the three. Knowing the approximate time span between these decays as well as their respective energies allows us to clearly identify alpha event triplets belonging to the same radon decay chain. The peaks corresponding to the alpha triplets can be seen in Figure 7. While not the goal of the experiment, this was to our knowledge the first time that acoustic power and frequency spectrum data were used to identify specific alpha decay events and their associated energies.
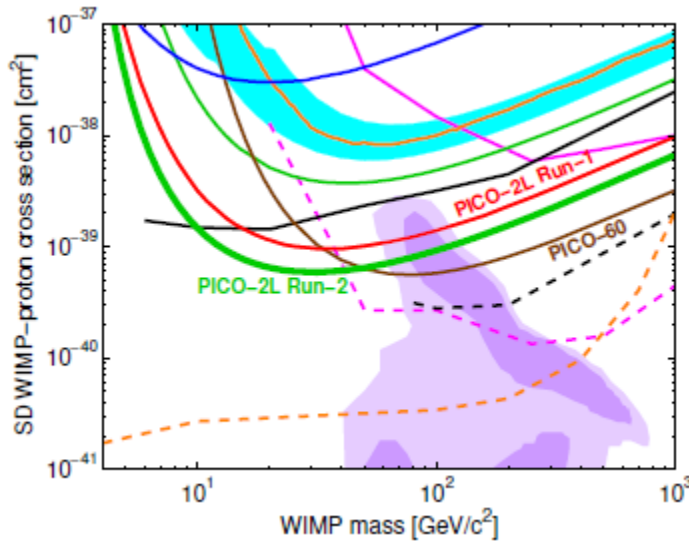
Figure 8. 90% C.L. limit on spin-dependent WIMP-proton cross section from various PICO runs (labeled) as well as other detectors such as XENON100 (orange) and SuperK (dashed/solid black).

PICO results have thus far been able to place further constraints on possible WIMP masses for both spin-dependent (see Figure 8) and spin-independent interactions. Bubble chamber technology remains the best detector type for spin-dependent dark matter direct detection, particularly with target fluids rich in elements such as fluorine with unpaired nucleons to contribute to the particle scattering. However, with one WIMP candidate in the improved run of PICO-2L (see Figure 9) and no WIMP candidates in the PICO-60 run, dark matter has thus far not been directly detected with any amount of confidence. Nevertheless, elimination of further background sources of bubble nucleation via higher quality materials and improved experimental methods is achieved with each subsequent run, and detector technology continues to advance, probing smaller WIMP-proton cross sections and larger mass ranges than ever before.

ACOUSTIC METHODS

Given the transient and microscopic nature of the events being studied, proper analysis of the data is of critical importance before any conclusion about dark matter can be drawn. While optical data has been used in previous analyses to distinguish wall events from the bulk events in which a dark matter signal would be expected, acoustic signal data is expected to be a more precise indicator of this and other event characteristics. Visual data are constrained by limitations such as camera resolution, shutter speed, and

Figure 9. Plot showing wall events (black dots), bulk events (blue circles), and WIMP candidate events (red dots) from run 1 (left) and run 2 of PICO-2L [10]

optical artifacts, while acoustic signals are strongest when the bubble is approximately 20 μm in diameter. This means that acoustics can theoretically convey information about regions less than 20 μm from the chamber wall – a considerable improvement over visual sensitivity.

In the first PICO-2L run, discrimination between wall and bulk events was not particularly dependable and a larger number of events were identified as possible WIMP candidates. After several improvements (such as meticulous particulate removal and better fiducial cuts), the second run yielded cleaner results with a much more defined demarcation between bulk and wall events, as can be seen in Figure 9. Also, the number of WIMP candidates identified decreased considerably. These results highlight the

14

importance of having the highest specificity cuts that are possible; ideally, no wall events should be misidentified as bulk events (thus being inadvertently included in the data as opposed to cut out) – a 100% specificity. More frequent false positives – i.e., bulk events being misidentified as wall events – equates to lower efficiency, as useful data is being discarded unnecessarily. Altering or combining the cuts used can increase efficiency at the expense of specificity (or vice versa). A cut with less than 100% specificity (but higher efficiency) can be used to cross-check the existing cuts being applied to the data. While the second PICO-2L run utilized improved optical reconstruction, acoustic data has the potential to be far more sensitive and precise in identifying bubble differences that may be indicative of wall versus bulk events, potentially resulting in a cleaner dark matter search data set.

The PICO collaboration uses Python software to help reconstruct, analyze, and review the events taking place within the chamber. Using the PICO Event Display, several dozen events were examined by hand to determine whether they were likely to be wall or bulk events based on existing visual criteria. The event display can pull up data variables such as run type, *pset*, *Dwall*, and t_0 values – all of which were used when hand-scanning for bulk and wall events. The run type classifies whether the bubble event occurred during dark matter search data, neutron calibration, or gamma calibration data. Bulk events were selected from either the dark matter search data or the neutron calibration data, as these are the background events expected to most closely resemble the anticipated dark matter particle. The *pset* value describes the

pressure setting of the target liquid at time of event capture; this variable was controlled for – only events at a *pset* of 30.0 PSI were used.

Using stereo images from the multiple cameras, reconstructed data is able to obtain a bubble's position within the chamber and, therefore, its distance from the chamber wall *Dwall* at t_0 in millimeters. This value was used as a cross-check after visually scanning through the images. Also, ideal bulk events were considered to be those bubbles which did not make contact with the jar wall at any point but also were reasonably close to the wall boundary (within ~50 mm). The intent of this was to control for any possible acoustic differences between bulk bubbles closer to the center of the jar and bulk bubbles nearer to jar boundaries that were not related to the mechanics of formation along the wall. Pressure rise data was also reconstructed to obtain a t_0 value – the time identified as the onset of the bubble event. Knowing this value facilitated in identifying the optimum frequency range at which to observe the power spectrum density plots of the events; knowing where on the graph bubble nucleation occurred allowed for easier demarcation between true bubble signal and background noise. The t_0 was also used to locate the time window of each event signal to use for consistency – ensuring the power spectrum density plots were only being obtained from the acoustic signals between event onset and a pre-designated length of time after t_0. 0.09 seconds was selected as a rough estimate, after which point the triggering of the chamber decompression became the dominant observable signal. Later in the analysis, this was refined to 0.08 seconds after t_0, when it was observed that several events were undergoing compression prior to the originally defined cutoff.

Once at least twenty events of each type (bulk and wall) were visually identified, additional Python software was used to plot the raw acoustic signal (showing the $t_0 - (t_0 + 0.09$ s) range). Filtering code was used to examine acoustic plots showing only certain frequency ranges. This was achieved by first applying a fast Fourier transform (FFT) of the

Figure 10. Graphs of three events from PICO-30L data: original acoustic signal (magenta), fast Fourier transform frequency spectrum below (green), average spectrum for three events (blue).

original acoustic signal, adding a cut to eliminate unwanted frequencies, then applying an inverse Fourier transform to yield a filtered acoustic signal. Events were examined at frequency ranges starting at 1 – 5 kHz until roughly 50 – 100 kHz. A visual inspection comparing the noise measured prior to t_0 to the bubble signal measured after t_0 suggested that between 3 and 20 kHz was a suitable frequency range for which to filter the raw data; background noise seemed minimal while bubble signal seemed strongest.

From there, the filtered and trimmed acoustic signal (3 − 20 kHz, within the time window), and the average power vs. time were also plotted for each event. Figure 10 compares plots for three events: the magenta plot is the raw acoustic signal, the green plot is the fast Fourier transform frequency spectrum of the corresponding magenta plot above, and the aqua plot is the average of the three green frequency spectra.
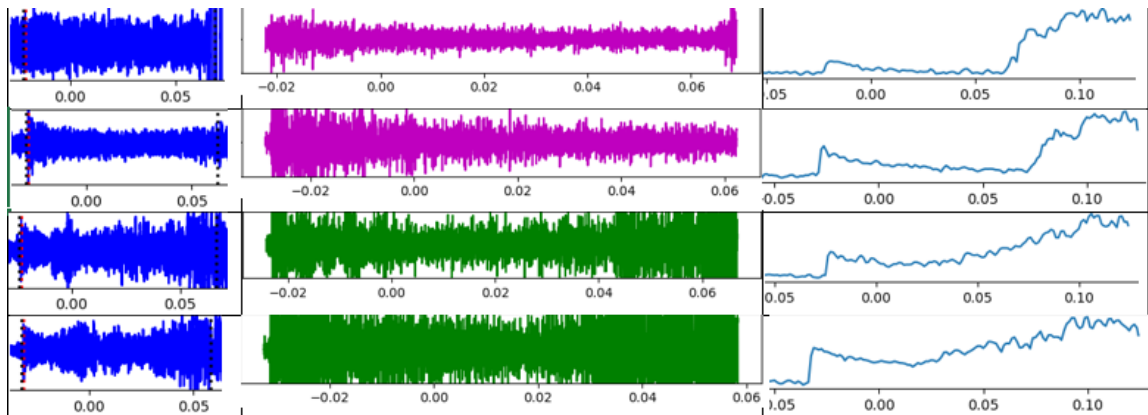
Figure 11. Filtered acoustic plots of two bulk events (magenta) and two wall events (green) with respective raw acoustic data to the left and corresponding average power vs. time plot to the right. Wall events can clearly be discerned both as louder overall and as having different characteristic power graph shapes.

Figure 11 gives a more complete picture using various plots for two bulk events (magenta) and two wall events (green). The plots on the left show raw acoustic data; the plots in the middle are acoustic data filtered for 3 − 20 kHz; the plots on the right show the average power vs time for each event.

Additional wall and bulk events were visually identified until there were roughly

40 of each. The Python code was subsequently configured to show average plots

(acoustic data, power spectrum density, and power vs time) for all bulk events and

similarly for all wall events. Comparison between the two sets allowed for distinguishing

features to be discerned. A shifted version of the power vs time plot was created to

account for the fact that the t_0 time was different for each event; the shifted plot moved

each event's t_0 to a central location and returned one average plot for all bulk and wall

events with t_0 values overlapping. These average plots indicated that wall events were

generally much louder (total power over the set interval) and took a shorter time to

reach minimum power after bubble nucleation. The ranges of this "max – min time" as

well as the ranges for power were checked to identify cut-off values to use as event

indicators. Values were chosen such that no wall-to-bulk mischaracterizations occurred;

that is, wall events being incorrectly identified as bulk events. Since wall events

mistakenly identified as bulk events can mimic a dark matter signal, it was important to
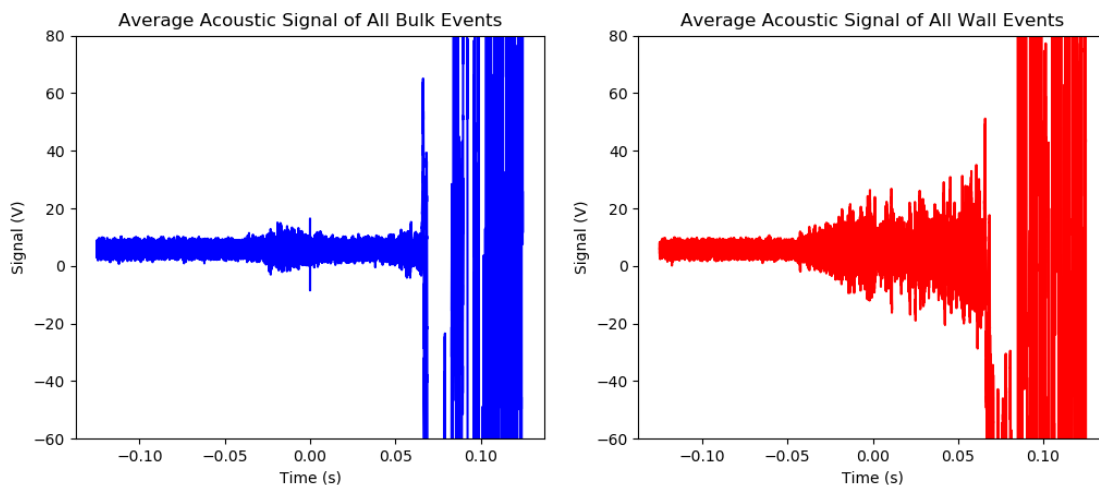
Figure 12. Average raw acoustic signal of all bulk (left) and wall events (right).

ensure the cuts did not inadvertently include wall events that would have otherwise

been excluded.

ACOUSTIC RESULTS

A spreadsheet of all bulk and wall events is included in the appendix: each event

is labeled with its number and other characteristics such as run type, *Dwall*, t_0; the three

plots of Figure 11; and a photo of the bubble from the last frame (when the bubble is

largest). Two bulk events were later removed from the data set when upon further

review, the images indicated that these could plausibly be wall events, and were

previously misidentified in error. Once calculated, the total power output of each event

(during the interval [$t_0 - 0.001$ s] to [$t_0 + 0.09$ s]) as well as the time taken for power

output to drop from its peak value at bubble nucleation to the minimum power right

before chamber compression (the aforementioned "max – min" value) were added to

the spreadsheet.

The range of these two values was noted between bulk and wall events. Bulk

event power varied between 1,780 – 23,953 in arbitrary units and "max – min" time

ranged from 0.0300 to 0.0975 s. Wall event power varied between 8,150 – 52,849 and

"max – min" time ranged from 0.0110 – 0.0675 s. The average power of a wall event

was found to be 18,069 – over four times larger than the average power of bulk events

(at 4,056).

Figure 12 compares the average raw acoustic signal from all bulk events (blue) and wall events (red). The stronger signal for wall events is easily identifiable. As noted previously, it can be visually discerned that wall events differ from bulk events in both overall loudness and power-vs-time graph shape. Figures 13 and 14 compare the
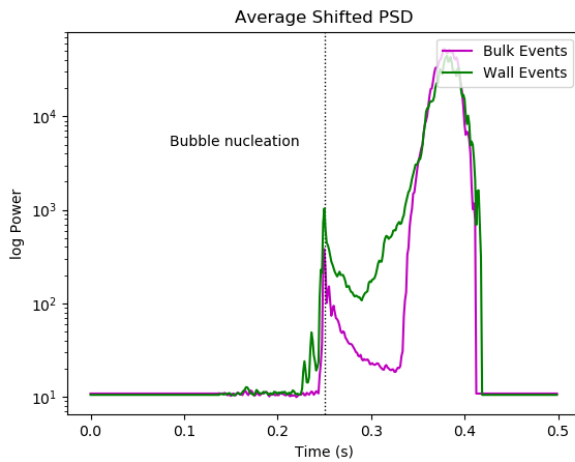
Figure 13. Average shifted power vs. time plot of all bulk (magenta) and wall events (green) at 3 − 20 kHz.

average shifted power-vs-time plot of all bulk (magenta) and wall (green) events. Bubble nucleation occurs at the dashed line; t_0 is at 0.25 seconds on every shifted plot. The large peaks on the right of each graph represent the loud compression stage. In between bubble nucleation and chamber compression are the distinct differences between events; the average wall event is considerably more powerful as can be seen by the larger area under the curve. Also, the power output does not drop as low for the average wall event as it does for bulk events just prior to compression.

The average frequency spectra were plotted and observed for bulk versus wall events as well. This was done to test whether wall events had visually different frequency distributions from bulk events and to ensure the 3 – 20 kHz range was optimal. The two plots showed few differences and both
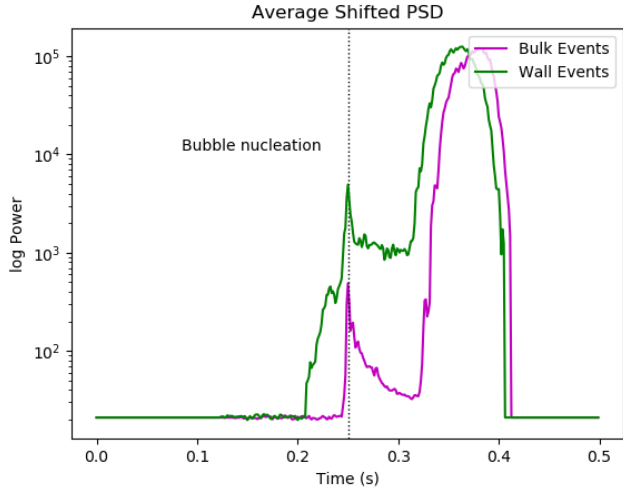
Figure 14. Average shifted power vs. time plot of all bulk (magenta) and wall events (green) at 1 - 75 kHz.

peaked in the 1 – 75 kHz range, indicating all events were most prominent at those frequencies. Therefore, a pair of average shifted power-vs-time plots were also created for the 1 – 75 kHz range, and can be seen in Figure 14. The plots are very similar to Figure 13 but with amplified differences between bubble nucleation and chamber compression; it is clearer from this plot that wall events are more powerful.
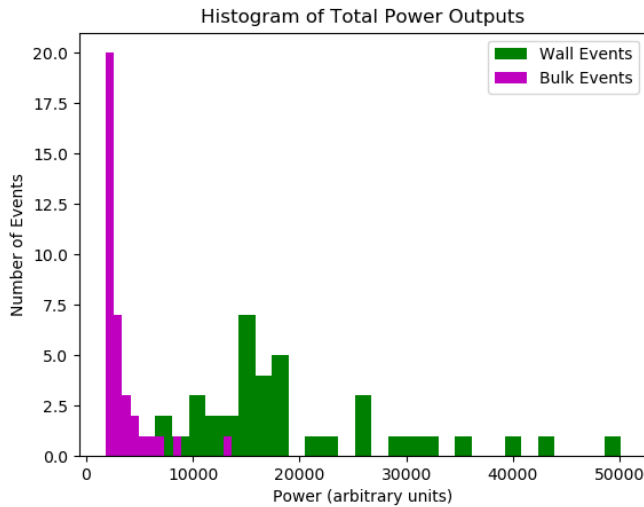
Figure 15. Histogram of total power outputs between [t0-.001] - [t0+.08] of all bulk (magenta) and wall events (green) at 3 - 20 kHz.

The first cut chosen to identify wall events acoustically was determined by an event's total power output. Figure 15 shows a histogram of wall (green) and bulk (magenta) event power outputs.

Almost all bulk events had total power output under 10,000 and the vast majority of those were below 5,000. Meanwhile, wall events have a mean power output between 15,000 and 20,000, and a much larger spread, with many events in the $20,000 - 50,000$ range. The power cut-off was placed at 6,400 for optimum specificity.

As there was considerable overlap between the "$max - min$" ranges, this was decided to not be used as a cut when differentiating between wall and bulk events. Instead, the slope of the line between the maximum and minimum power values was calculated for each event (and added to the spreadsheet) by pulling the power value at these locations, taking the difference, and dividing this by the "$max - min$" time interval. This power $max - min$ slope was found to be a better indicator of event type: bulk event slopes ranged from -1,363 to -31,337 while wall event slopes ranged from -6,512 to -103,943. Figure 16 shows a histogram of wall (green) and bulk (magenta) power $max -$ min slopes. With the exception of a handful of events, there was no overlap between these ranges. Bulk events have less negative slopes, almost all of which were between -10,000 and 0. Wall events have a mean power $max - min$ slope around -20,000 and a much larger spread with more negative values. It became apparent that this power max

– min slope, along with the total power output of an event were the best variables to use for subsequent cuts.

Given a power cut-off of 6,400, zero wall events were misidentified as bulk and 3 of 37 bulk events were misidentified as wall events. This gives the power cut alone a specificity of 100% and an efficiency of 92%. Using a power max – min slope cut-off of -6,500, zero wall events were misidentified and 6 bulk events were mischaracterized as

wall events. This cut alone yields a specificity of 100% and an efficiency of 84%. Combining and loosening the cuts was found to greatly increase efficiency; the Python code was altered to declare wall events as those with greater than 11,000 total
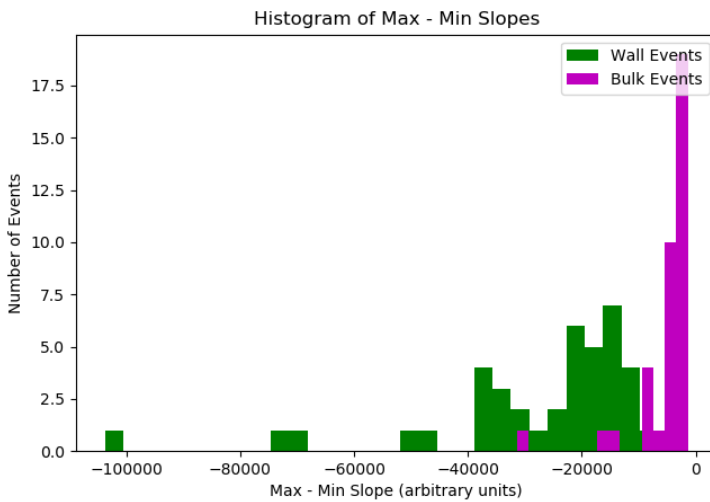
Figure 16. Histogram of power max – min slopes of all bulk (magenta) and wall events (green) at 3 - 20 kHz.

power AND a power max – min slope less than -9,500. This resulted in four wall events being misidentified as bulk events – an unfavorable result for specificity – but only one bulk event being misidentified as a wall event. The combined cuts yield a specificity of 90% and an efficiency of 97%.

To obtain a visual representation of the variables used, a 2-dimensional scatter plot showing max – min slope vs the log of the power values for each event was created. This is shown in Figure 17, with bulk events represented as magenta circles and wall

24

events as green circles. No clear linear cut is discernible that would be of greater efficiency or specificity than the previous cuts made (which can be represented as vertical and horizontal lines on the scatter plot). However, it can be noted that bulk events are more tightly clustered along the trend line (not pictured), whereas wall events have a greater spread – especially at higher powers.
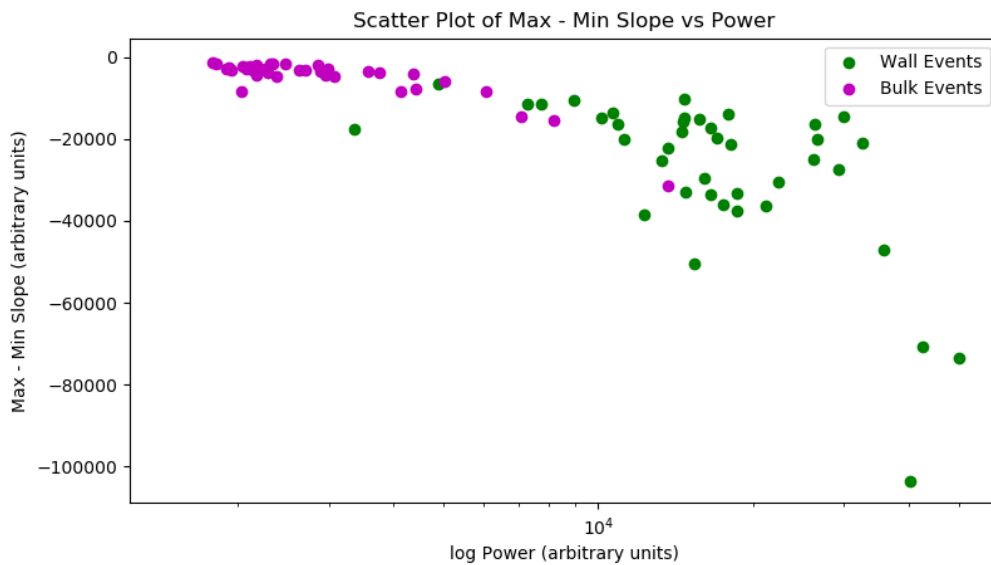
Figure 17. 2D scatter plot of max - min slope vs log of power for each event; bulk events as magenta circles, wall events as green circles.

The average power spectral density (log of power vs log of frequency) was also plotted for bulk (magenta) and wall events (green) and then smoothed using a Savitzky-Golay filter. This plot – shown in Figure 18 – confirms that wall events are consistently more powerful than bulk events in the 1 – 75 kHz range.

DISCUSSION

Although this analysis is tested with low statistics (40 wall events and 37 bulk events), the preliminary efficiencies and specificities of the cuts indicate that bubble chamber acoustics are a powerful independent variable that can be used to complement the existing fiducial cuts. As the spreadsheet of results in the appendix shows, nearly every wall event has a power vs. time plot that is distinguishable from nearly every bulk event. This shows that there are noticeable differences between event types even prior to performing any statistical analysis. These early results suggest that acoustic cuts, when combined with the existing cuts on the dark matter search data, will yield a cleaner data set with more true wall events being

Figure 18. Average power spectral density vs frequency for wall (green) and bulk events (magenta).

identified as such and fewer bulk events being misidentified as wall events (and, thus, thrown out of the search data).

Combining the power max – min slope and power cuts on the acoustic data allows for loosening of the cut-off values while still having improved efficiency. Modifying the cut-off values will alter the specificity and efficiency, which can also be used as a cross-check on existing cuts.

Based on this initial research, the piezo-electric acoustics data obtained from bubble events within the PICO bubble chamber appear to be useful in identifying whether an event formed on the wall of the chamber or within the bulk of the superheated liquid. This serves as an important tool when making cuts in the dark matter search data, which can theoretically allow for improvement of the possible WIMP-proton cross sections and mass ranges.

BIBLIOGRAPHY

[1] Adam, R. et al. "Planck 2015 Results. I. Overview of Products and Scientific Results." ArXiv, 2015, doi:10.1051/0004-6361/201527101.

[2] Undagoitia, Teresa Marrodán, and Ludwig Rauch. "Dark Matter Direct-Detection Experiments." Journal of Physics G: Nuclear and Particle Physics, vol. 43, no. 1, 2015. Crossref, doi:10.1088/0954-3899/43/1/013001.

[3] Knox, L. "The Value of Planck CMB Temperature Maps in a Post-WMAP World." Lloydeknox, 21 July 2015, www.lloydknox.com/single-post/2015/07/21/The-Value-of-Planck-CMB-Temperature-Maps-in-a-postWMAP-World.

[4] Amole, C. et al. "Dark Matter Search Results from the PICO-2L C3F8 Bubble Chamber." Physical Review Letters, 2015, arxiv.org/abs/1503.00008.

[5] Lea, R. "Dark Matter: Taking a Closer Look at the (Un)usual Suspect", Astronomy, 20 January 2021, www.astronomy.com/news/2021/01/dark-matter-the-unusual-suspects

[6] Baudis, L. "Direct Dark Matter Detection: The next Decade." Physics of the Dark Universe, vol. 1, no. 1–2, 2012. Crossref, doi:10.1016/j.dark.2012.10.006.

[7] Amole, C. et al. "Dark Matter Search Results from the PICO-60 CF3I Bubble Chamber." Physical Review D, 2015, arxiv.org/abs/1510.07754.

[8] Amole, C., et al. "Dark Matter Search Results from the PICO-60 C3F8 Bubble Chamber." Physical Review Letters, 2017, arxiv.org/abs/1702.07666.

[9] Amole, C. et al. "Dark Matter Search Results from the Complete Exposure of the PICO-60 C3F8 Bubble Chamber." Physical Review D, 2019, arxiv.org/abs/1902.04031.

[10] Amole, C., et al. "Improved Dark Matter Search Results from PICO-2L Run 2." Physical Review D, 2016, arxiv.org/abs/1601.03729.

[11] Bressler, M. et al. "A Buffer-Free Concept Bubble Chamber for PICO Dark Matter Searches." ArXiv, 2019, arxiv.org/abs/1905.07367.
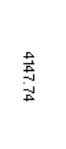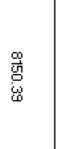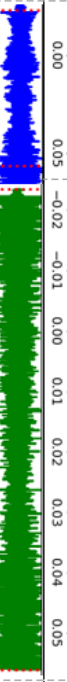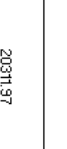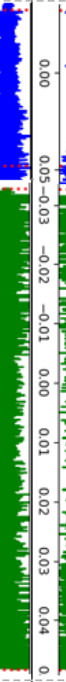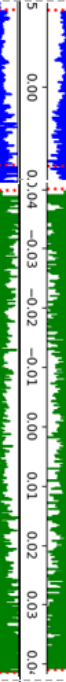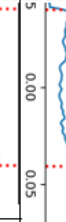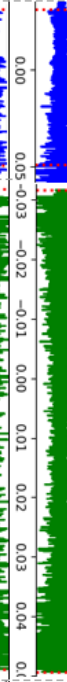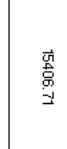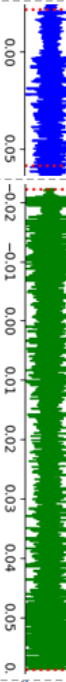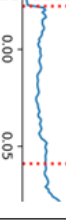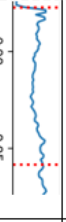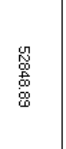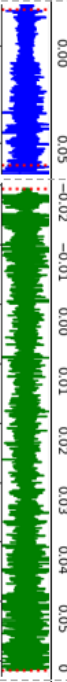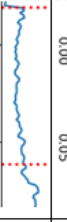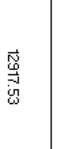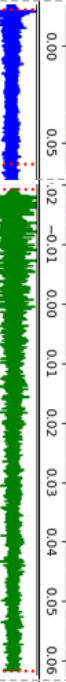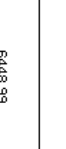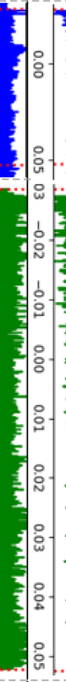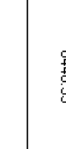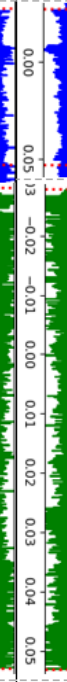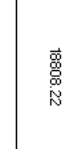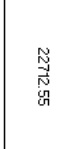
[12] Amole, C. et al. "Data-Driven Modeling of Electron Recoil Nucleation in PICO C3F8 Bubble Chambers." Physical Review D, 2019, arxiv.org/abs/1905.12522.
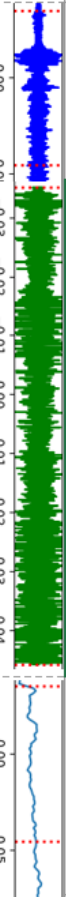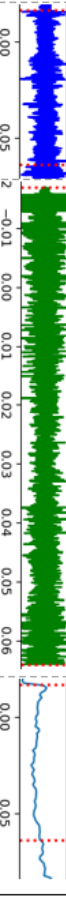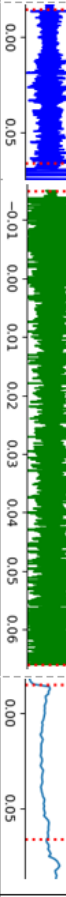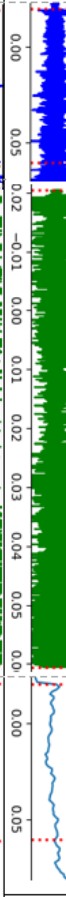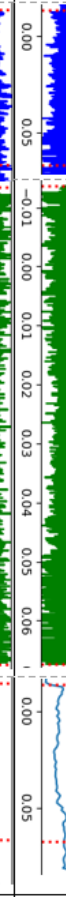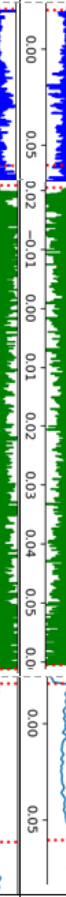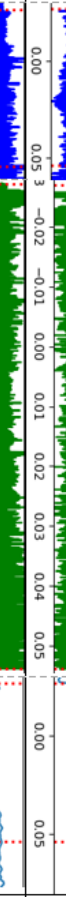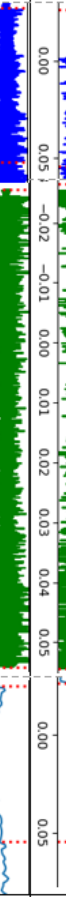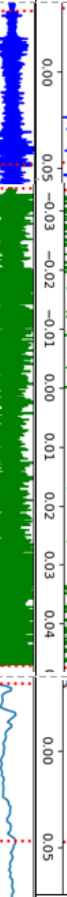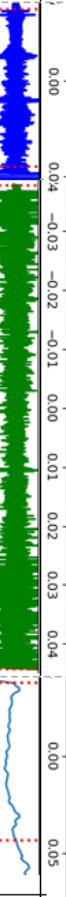
Event Type	Run #	Event #	Run Type	Dwell	t0	Raw Acoustic Signal	Filtered (3 - 20 kHz) Acoustic Signal (trimmed, ±35V)	Window Avg PSD	Total power ([t0-.001] - [t0+.08])	Max - min time (s)	Max - min power	Max - min Slope	PED Image (cam #)
Bulk	20161109_3	23	14	15.28	-0.03				2036.49	0.0625	133.6	-2137.6	2
Bulk	20161109_3	2	14	10.98	-0.01				2311.04	0.065	95	-1461.5	2
Bulk	20161109_2	9	14	18.79	-0.01				1901.47	0.0612	172.9	-2825.2	2
Bulk	20161109_0	18	14	12.44	-0.03				2110.48	0.085	177.3	-2085.9	4
Bulk	20161109_0	4	14	12.32	-0.02				2171.74	0.0562	237.9	-4233.1	2
Bulk	20161109_0	1	14	13.04	-0.03				1938.41	0.06	183.3	-3055.0	2
Bulk	20161108_5	17	14	16.24	-0.02				1773.55	0.0875	119.3	-1363.4	2
Bulk	20161108_3	43	14	15.20	-0.01				2621.19	0.0775	247.8	-3197.4	4
Bulk	20161108_3	13	14	19.61	-0.01				2889.98	0.0787	282.1	-3584.5	2
Bulk	20161108_3	8	14	17.14	-0.03				2027.93	0.03	251.6	-8386.7	2
Bulk	20161108_2	47	14	11.36	-0.02				2256.26	0.0688	204.9	-2978.2	4
Bulk	20161108_2	37	14	17.04	-0.02				2858.12	0.0787	159.3	-2024.1	1

Bulk	20161004_	40	10	5.63	-0.03	[plot]	[plot]	[plot]	8202.2	0.0737	1137.6	-15435.5	[image]
Bulk	20161202_	43	10	22.47	-0.02	[plot]	[plot]	[plot]	2476.3	0.0762	124.4	-1632.5	[image]
Bulk	20161202_	35	10	21.52	-0.03	[plot]	[plot]	[plot]	2070.13	0.0737	193.4	-2624.2	[image]
Bulk	20161202_0	34	10	21.52	-0.02	[plot]	[plot]	[plot]	2054.24	0.0687	239.8	-3490.5	[image]
Bulk	20161202_1	12	10	21.74	-0.02	[plot]	[plot]	[plot]	2166.1	0.08	140.5	-1756.3	[image]
Bulk	20161201_1	47	10	5.73	-0.04	[plot]	[plot]	[plot]	2989.68	0.0975	267.9	-2747.7	[image]
Bulk	20161108_4	6	14	18.96	-0.02	[plot]	[plot]	[plot]	13851.67	0.0788	2463.4	-31337.6	[image]
Bulk	20161109_6	39	14	11.63	-0.03	[plot]	[plot]	[plot]	2289.63	0.07	268.2	-3831.4	[image]
Bulk	20161109_5	45	14	15.81	-0.02	[plot]	[plot]	[plot]	1813.23	0.0925	135.8	-1468.1	[image]
Bulk	20161109_5	11	14	17.10	-0.02	[plot]	[plot]	[plot]	1914.96	0.065	158	-2430.8	[image]
Bulk	20161109_5	2	14	15.20	-0.02	[plot]	[plot]	[plot]	2140.2	0.0587	191.8	-3267.5	[image]
Bulk	20161109_4	22	14	12.24	-0.03	[plot]	[plot]	[plot]	2075.93	0.0862	238.9	-2771.5	[image]
Bulk	20161109_3	36	14	10.05	-0.03	[plot]	[plot]		2380.09	0.0437	208.8	-4778.0	[image]

ID									
Bulk 20161205_2	28	10	10.74	-0.02	4364.93	0.0825	330.6	-4007.3	4
Bulk 20161205_6	25	10	5.09	-0.02	2960.34	0.0875	375.1	-4286.9	4
Bulk 20161207_2	33	10	9.19	-0.01	3067.5	0.0575	269.5	-4687.0	3
Bulk 20161209_0	48	10	11.37	-0.02	3577.38	0.0775	261.7	-3376.8	1
Bulk 20161209_	0	10	9.24	-0.02	5044.94	0.0825	495	-6000.0	2
Bulk 20161209_	42	10	5.12	-0.02	11470.11	0.0825	2151.9	-26083.6	4
Bulk 20161212_1	25	10	5.19	-0.02	23952.51	0.05	2278.2	-45564.0	2
Bulk 20161213_0	2	10	26.66	-0.02	4416.48	0.0788	618.5	-7849.0	4
Bulk 20161213_0	26	10	5.25	-0.02	7101.11	0.0812	1167.7	-14380.5	2
Bulk 20161213_1	55	10	8.88	-0.03	3769.16	0.0712	270.4	-3737.8	1
Bulk 20161215_1	28	10	7.19	-0.02	6053.27	0.0788	664	-8426.4	1
Bulk 20161216_0	50	10	21.24	-0.03	2694.33	0.085	262	-3082.4	2
Bulk 20161217_0	28	10	20.78	-0.03	2330.88	0.09	157.8	-1753.3	4

Type	Date	ID				Blue plot	Green plot	Blue plot					Image
Bulk	2016127_0	31	10	20.86	-0.02				4147.74	0.0625	522.7	-8363.2	
Wall	20161201_0	0	10	0.95	-0.02				8150.39	0.0275	310.7	-11298.2	
Wall	20161213_1	57	10	0.22	-0.03				20311.97	0.0462	762.1	-16495.7	
Wall	20161213_1	58	10	1.10	-0.04				20432.02	0.0325	649.4	-19981.5	
Wall	20161213_1	59	10	0.61	-0.03				15406.71	0.0338	586.9	-17363.9	
Wall	20161213_1	60	10	3.56	-0.02				17451.36	0.0412	571.5	-13871.4	
Wall	20161213_1	62	10	2.29	-0.02				52848.89	0.0425	3118.7	-73381.2	
Wall	20161214_0	1	10	0.66	-0.02				12917.53	0.0425	446.2	-10438.8	
Wall	20161214_0	2	10	-0.79	-0.03				6448.99	0.0675	1197	-17733.3	
Wall	20161214_0	3	10	-0.42	-0.03				18808.22	0.0387	1147.6	-29653.7	
Wall	20161214_0	4	10	0.69	-0.03				22712.55	0.0475	1305.4	-27482.1	
Wall	20161214_0	6	10	1.57	-0.03				24071.73	0.0112	531.2	-47428.6	
Wall	20161214_0	8	10	0.26	-0.01				12997.41	0.0562	834.7	-14852.3	

Wall	ID (20161214_0)	n	val1	val2	Sum	Mean	SD?	Min?
Wall	36	10	0.82	-0.03	6620.05	0.0925	602.4	-6512.4
Wall	32	10	-157	-0.02	19254.89	0.0387	1400.9	-36199.0
Wall	31	10	-0.22	-0.04	32272.58	0.0262	2723.3	######
Wall	26	10	0.14	-0.03	12252.8	0.045	673.7	-15104.4
Wall	25	10	0.96	-0.03	22777.84	0.0288	717.7	-24920.1
Wall	23	10	0.22	-0.03	19726.62	0.0275	906.7	-32970.9
Wall	22	10	0.66	-0.02	13739.97	0.0425	940.1	-22120.0
Wall	21	10	-179	-0.01	20269.06	0.0312	511.2	-16384.6
Wall	19	10	4.88	-0.03	24199.7	0.04	836.9	-20922.5
Wall	18	10	-0.38	-0.02	24389.62	0.0338	1229.7	-363817
Wall	17	10	0.14	-0.01	19883.88	0.0225	846	-376000.0
Wall	13	10	-0.31	-0.02	14697.94	0.0387	1487.5	-38436.7
Wall	10	10	2.00	-0.03	18541.86	0.0187	622.6	-33294.1

Wall	Wall	Wall	Wall	Wall	Wall	Wall	Wall	Wall	Wall	Wall	Wall	Wall
20161216_	20161216_	20161216_	20161216_	20161216_0	20161216_0	20161216_0	20161201_0	20161201_0	20161214_0	20161214_0	20161214_0	20161214_0
6	4	3	0	55	54	53	1	0	46	45	40	38
10	10	10	10	10	10	10	10	10	10	10	10	10
-17	-12	-0.5	0.08	2.81	0.32	-0.3	0.73	0.95	1.37	0.89	0.98	0.80
16721.08	17083.81	15921.08	16559.36	30732.52	13983.31	21275.81	15139.58	8150.39	14662	16531.96	14316.69	11139.96
0.0375	0.0137	0.0338	0.0562	0.0362	0.0375	0.0325	0.0375	0.0275	0.0387	0.03	0.0387	0.0387
796.5	692.3	460.2	1020.7	2567.1	948.1	986.5	745.5	310.7	564.5	1008.5	577.3	393.6
-212140.0	-505328	-13615.4	-18161.9	-70914.4	-252282.7	-303353.8	-198800.0	-112398.2	-145866.6	-33616.7	-14317.3	-10170.5

Wall	Wall
20161216_1	20161216_1
9	10
10	10
0.34	-0.1
-0.02	-0.04
14824.79	14519.53
0.05	0.0412
998.9	652.8
-13978.0	-15844.7